Pure & Appl. Chem., Vol. 62, No. 12, pp. 2251–2258, 1990.
Printed in Great Britain.

Diffraction and X-ray absorption studies of electrolyte solutions

Toshio Yamaguchi

Department of Chemistry, Faculty of Science, Fukuoka University, Nanakuma, Jonan-ku, Fukuoka 814-01, Japan

Abstract - Microscopic structures of electrolyte solutions over a wide range of concentration have been determined by three different techniques; X-ray diffraction, neutron diffraction combined with isotopic and isomorphic substitution, and X-ray absorption methods. Advantages and limitations in structural information obtained by the three methods are briefly described. The structures of some ionic solutions in room temperature liquid, undercooled, and glassy states have been revealed from comparative X-ray and neutron diffraction and X-ray absorption measurements. Physico-chemical data of the solutions are discussed from the microscopic structures of the solutions.

1. INTRODUCTION

Most of chemical reactions in nature, synthetic industry, biological systems, etc. occur in aqueous or non-aqueous solutions. The mechanisms of the reactions and the properties of solutions depend upon the ion-solvent, solvent-solvent, and ion-ion interactions; these interactions manifest themselves in the microscopic structure of the solutions. Thus the structure of electrolyte solutions, in particular, of solvated ions and chemical species involved in the reactions, is essential in understanding the reactions and the physico-chemical quantities of the solutions.

According to Braunstein (1), the electrolyte solutions may be classified into five categories depending on the water content; (I) very dilute solution, (II) concentrated aqueous solution, (III) hydrate melts, (IV) melts containing incompletely hydration sheaths, and (V) anhydrous molten salts. Most of structural studies so far reported have been devoted to categories II and V. On the contrary, there appeared very few structural investigations on I, III, and IV.

The solutions in category I have been mostly used for thermodynamic studies; thus structural information will play a key role in interpreting thermodynamic parameters of chemical reactions in the solutions. On the other hand, the electrolyte solutions in categories III and IV are of considerable interest both from fundamental chemistry such as crystallization of the salts and supercooling of the solutions, and from technological applications as thermal energy storage (2).

Among various techniques so far developed, X-ray diffraction method has long been used for structure determination of liquids and solutions (3). Neutron diffraction method has also been proved to be very successful when it is combined with isotopic substitution method (4). With the progress of synchrotron radiation X-ray absorption spectroscopy has become one of the powerful means for structural studies of electrolyte solutions (5). In addition, intense white X-rays available at synchrotron radiation facilities have made it possible to use the X-ray anomalous scattering technique for determination of the structure of solutions (6).

The above three techniques are superior to other methods because they give us *direct* structural information related to the radial distribution of atom pairs in a system; the number of neighboring atoms around a central ion, the interatomic distances between them, and its root-mean-square deviation. It is timely to discuss the advantages and limitations of each technique and their applications to structural studies of electrolyte solutions.

2. STRUCTURE DETERMINATION

The structure of an electrolyte solution is expressed in terms of one-dimensional pair correlation function (radial distribution function). In case solute MX_n is dissolved in water the total radial distribution function $G(r)$ for the solution consists of ten partial distribution functions (for a simplicity the weight of each $g(r)$ is omitted).

$$\begin{aligned} G(r) &= g_{MO}(r) + g_{MH}(r) + g_{XO}(r) + g_{XH}(r) && (ion\text{-}solvent) \\ &+ g_{MM}(r) + g_{XX}(r) + g_{MX}(r) && (ion\text{-}ion) \\ &+ g_{OO}(r) + g_{OH}(r) + g_{HH}(r) && (solvent\text{-}solvent) \end{aligned}$$

For structural determination of the solution our aim is thus to derive the individual $g(r)$s from experiments. In the total $G(r)$, which is obtained by a conventional diffraction measurement, are superimposed the peaks of the ten partial $g(r)$s (see Fig. 1(a) and (b)); thus it is often difficult to uniquely determine the structure of solution. In particular, in a very dilute solution, the solvent-solvent interaction is predominant and the contributions of the ion-solvent and ion-ion interactions are at the background level in intensity. In principle, we could derive ten individual $g(r)$s from ten independent experiments, however, such experiments are practically impossible.

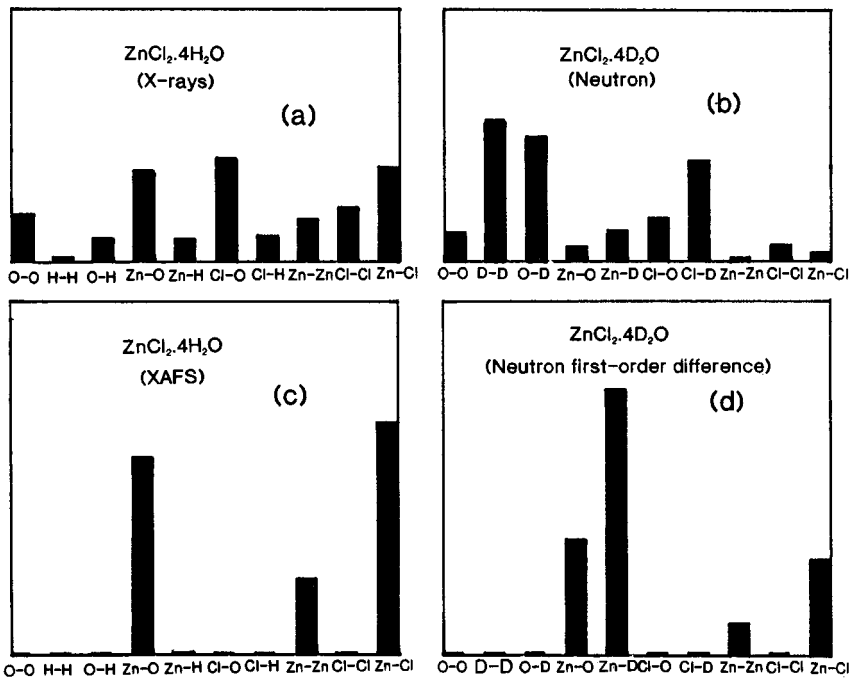

Fig. 1 Relative weightings of the partial g(r)s of a solution of $ZnCl_2.4H_2O$ for (a) X-rays, (b) neutrons, (c) XAFS, and (d) neutron first-order difference.

To overcome the above difficulty associated with the total $G(r)$ and to derive the ion-solvent and ion-ion interactions, X-ray anomalous scattering, neutron diffraction combined with isotopic or isomorphous substitution, and X-ray absorption fine structure method have been developed in the last decade. Details of the theories and techniques of the three methods have been described elsewhere (4,5,6).

The X-ray anomalous scattering method and the neutron diffraction with the substitution method both employ the difference technique that the pair interactions not related to an atom of interest are canceled out by taking the difference between two experimental data for two sample solutions with the same composition but with different X-ray form factors (or neutron scattering lengths) of the atom.

When two energies or two isotopes with different scattering lengths of atom M are used and the difference method is employed, we can get

$$G'_M(r) = g_{MO}(r) + g_{MH}(r) + g_{MM}(r) + g_{MX}(r) \qquad (2)$$

Similarly, for atom X we obtain

$$G'_X(r) = g_{XO}(r) + g_{XH}(r) + g_{XX}(r) + g_{XM}(r) \qquad (3)$$

It should be noted that the $G'_M(r)$ or $G'_X(r)$ contains only the pair distribution function related to atom M or X of interest, respectively, without the contribution from the solvent structure and the counter ions (see Fig. 1(d)). In the diffraction methods, the radial distribution function is related to the structure function $i(Q)$ through the Fourier transform,

$$i(Q) = (4\pi\rho/Q)\int (G'(r)-1)r \sin(Qr)dr \tag{4}$$

Here the momentum transfer Q is $4\pi\sin\theta/\lambda$, λ the wavelength, 2θ the scattering angle, ρ the number density of solution.

On the other hand, X-ray absorption spectroscopy does not require the difference technique and give structural information concerning absorbing atom M (or X) directly from a single experiment (see Fig. 1(c)). On an assumption of the single scattering theory, we have XAFS interference function $X(k)$ as

$$X(k) = \sum F_j(k)/kS_0^2(k)\int \exp(-2r_j/\lambda)\sin(2kr_j+\delta_j(k))P(r_j)/(r_j^2)dr_j \tag{5}$$

where k is the wave vector of the photoelectron, $F_j(k)$ the backscattering amplitude of the j-th atom, δ_j the phase shift, λ the mean free path of the photoelectron, and the $S_0^2(k)$ includes the multielectron process. Now, the term $F_j(k)\exp(-2r_j/\lambda)S_0^2(k)$ and $\delta_j(k)$ are corrected for a standard sample of known structure and $P(r)=4\pi\rho r^2 g(r)$, equation (5) can be rewritten as

$$X(k) = 4\pi\rho/k\int g(r)\sin(2kr)dr \tag{6}$$

From a comparison of eq.(6) with eq.(4), we can understand that both diffraction and XAFS methods give similar structural information.

Figure 2 shows the radial distribution functions obtained by the XAFS and diffraction methods. As seen in the figure, the radial distribution function obtained by the XAFS method is limited only to the short-range structure, usually to the first coordination sphere. This is inherent in the XAFS method since the XAFS interference function $X(k)$ is lack, due to the absorption edge, of the small k region containing information of the long-range ordering. The range used in the Fourier transform in eqs. (4) and (6) is critical for the resolution of the radial distribution function; the higher resolution is obtained the wider k-range is used. For the X-ray anomalous scattering technique the maximum Q value available in experiments is usually less than 10 $Å^{-1}$, thus a less pronounced distribution curve results (6).

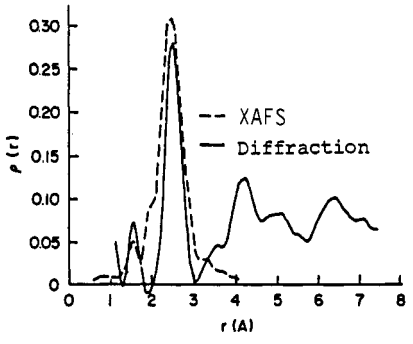

Fig. 2. Comparison of the radial distribution functions from XAFS and diffraction methods.

In spite of the above disadvantage of the XAFS method the technique has a great advantage for structure determination of a very dilute system, to which the diffraction methods are not practically applicable, when the fluorescent mode of measurement is employed rather than the conventional transmission mode. In addition, the near edge structure in XAFS contains information on electronic structure of ion, also giving evidence for the structure of chemical species in solution.

In eqs. (2) and (3) the terms related to the hydrogen atom, $g_{MH}(r)$ and $g_{XH}(r)$, are hardly seen with the techniques using X-rays because of small scattering factor of a hydrogen atom. On the contrary, the relative scattering length of a deuterium atom (in neutron diffraction the deuterium atom is used instead of a hydrogen atom because of large incoherent scattering cross section of the latter) is comparable with those of heavy metals. Thus, only the neutron diffraction method can reveal the structure involving hydrogen atom, e.g. the orientational correlation of water molecules (4).

3. RESULTS AND DISCUSSION

3.1 Very dilute solution – category I

In solution chemical species are in equilibrium and the quantity of each species can be accurately estimated by using the stability constants of the system. Since only an average structure of all chemical species present in solution is seen from the diffraction and X-ray absorption data, it is essential to know the composition of the species prior to structural experiments. For a complex equilibrium system, thus it is ideal to perform structural determination in the same system as used for the measurement of thermodynamic data.

Fluorescent X-ray absorption spectroscopy has been applied to copper(II) chloride - acetonitrile solutions with the total copper(II) concentration of 10 mM (M=mol dm^{-3}) (8), for which thermodynamic data have recently been measured (9). Figure 3 shows the distribution diagram of the copper(II) chloride complexes calculated from thermodynamic data. X-ray absorption spectra were measured around the Cu*K*-edge using synchrotron radiation. Sample solutions A, B, C, D, and E contain, respectively, solvated, mono-, di-, tri-, and tetrachloro complexes of Cu(II) ion.

In Fig. 4 X-ray absorption near-edge spectra of the copper(II) complexes show a systematic change in the spectral patterns with successive coordination of chloride ions to a central Cu(II) ion, reflecting the change in the electronic state of the complexes. The spectra will be interpreted in detail from molecular orbital calculations.

Figure 5 shows the Fourier transforms of samples A-E (not corrected for the phase shifts). The first peak is ascribed to interactions between a copper(II) ion and nearest neighbour atoms bound to it. The position of the peak shifts to the longer distance side with formation of copper(II) chloride complexes; the result shows that acetonitrile molecules coordinated to a copper(II) ion are replaced with chloride ions with an increase in chloride ion concentration. For the lower chloro complexes are observed the peaks ascribed to non-bonding Cu···C and Cu···C(CH_3) interactions within the copper(II)-acetonitrile interactions.

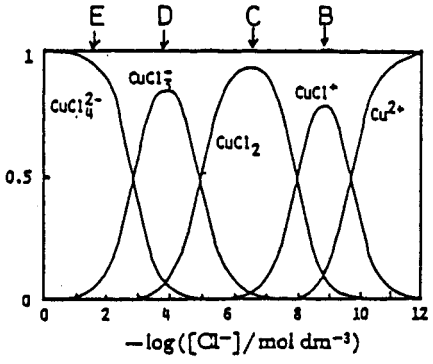

Fig. 3. Distribution curves of the copper(II) chloride complexes in acetonitrile solutions.

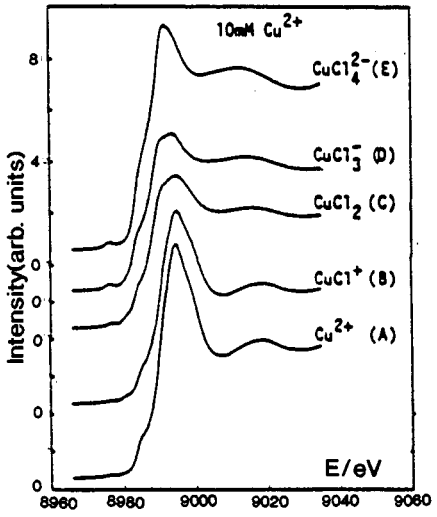

Fig. 4. X-ray absorption near-edge spectra of the copper(II) chloride complexes in acetonitrile solutions.

Structural parameter values of the stepwise Cu(II) species are summarized in Table 1 with thermodynamic quantities. We will now dicuss the thermodynamic parameters on the basis of the structures revealed. Stepwise enthalpies ΔH_n° (n=1-4) are all negative, in particular largely negative for n=4, while the stepwise entropy ΔS_n° is largely positive for n=1-3, but largely negative for n=4. These changes in the values from the trichloro- to the tetrachloro complex can be explained from the structure of the trichloro copper(II) complex. As seen in Table 1 the Cu-N bond length within the trichloro complex is surprisingly long, compared with those within the lower chloro complexes, showing an extremely weak solvation of an acetonitrile molecule to Cu(II) ion. Thus the formation of the tetrachloro complex is practically subject only to the bonding of a chloride ion to the trichloro complex with much less energy to break the Cu-N bond, resulting in the large negative ΔH_4° and ΔS_4°. The Cu-Cl bond length of 2.23 Å for the tetrachloro complex is very close to a mean Cu-Cl distance within $[CuCl_4]^{2-}$ of D_{2d} symmetry in $CsCuCl_4$ crystals.

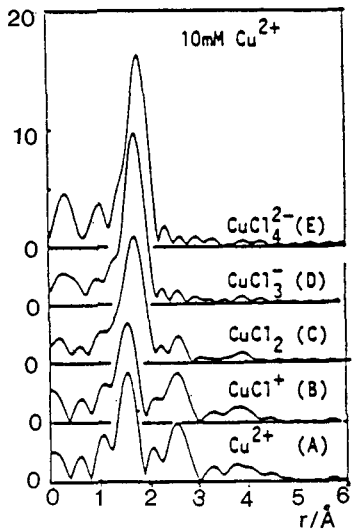

Fig. 5. Fourier transforms of the copper(II) chloride complexes in acetonitrile solutions.

Table 1. Structural parameters and thermodynamic data (9) of the copper(II) chloride complexes in acetonitrile solutions. r and σ are the interatomic distance (Å) and the Debye-Waller factor ($Å^2$), respectively.

	Cu - N		Cu - Cl				
	r/Å	σ/Å	r/Å	σ/Å	ΔG^a	ΔH^a	ΔS^b
$Cu(AN)_4^{2+}$	1.98	0.062	----	----	----	----	----
$CuCl(AN)_3^+$	1.97	0.055	2.18	0.092	-55.3	-11.7	147
$CuCl_2(AN)_2$	2.01	0.085	2.18	0.075	-45.4	-5.0	135
$CuCl_3(AN)^-$	2.19	0.19	2.17	0.069	-28.2	-4.4	80
$CuCl_4^{2-}$	----	-----	2.23	0.062	-16.3	-34.3	-61

[a] kJ/mol. [b] J/(K mol).

3.2 Liquid and glassy solutions – category III and IV

Undercooled and glassy solutions are in the metastable state between liquids and crystals. Thus, the structure of solutions in the metastable states will be important to understand the crystalization process and glassy transition. Glassy solutions have often been used in Mössbaur and ESR spectroscopies, however, the details of the change in chemical equilibria and structure in the vitrification process are ambiguous. We have recently performed X-ray and neutron diffraction and X-ray absorption measurements of solutions at liquid and glassy states of copper(II) acetate (10), copper(II) perchlorate (12), lanthanide(III) perchlorate (12,13,14), zinc(II) halides (15,16,17), and gallium(III) halides (16). Some examples are described below.

The hydration number of the lanthanide(III) ions has been discussed among various groups, in particular whether or not the hydration number changes in the series. The neutron diffraction measurements coupled with the isomorphous substitution method have been performed with perchlorate solutions of Pr(III)/Nd(III), Tb(III)/Dy(III), and Tm(III)/Yb(III) (13,14). A typical radial distribution function is shown in Fig. 6 for the solution of Tm(III)/Yb(III). The structural parameters are given in Table 2. It should be mentioned that the present results obtained by the isomorphous displacement are in good agreement within experimental accuracies with those by the isotopic substitution method (18,19,20). As seen in Table 2 the hydration number decreases from the light lanthanide ion to the heavy ions. The water molecules bound to the ions are tilted by about 20° in θ (Fig. 6), indenpedent on the series.

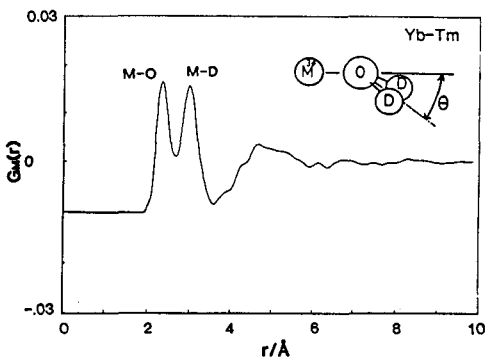

Fig. 6. The radial distribution function, $G_M(r)$, for 2.56 molal solutions of Tm(III) and Yb(III) perchlorates in heavy water(13).

Table 2. Interatomic distances (Å) and the hydration number (N) of aqua lanthanide(III) ions obtained from neutron diffraction and XAFS methods for aqueous lanthanide(III) perchlorate solutions

	Neutron			XAFS			
				Liquid		Glass	
	r_{MO}/Å	r_{MD}/Å	N	r_{MO}/Å	N	r_{MO}/Å	N
Nd	2.48	3.14	10	2.51	9.5	2.51	9.6
Sm	....	....	..	2.45	9.3	2.45	8.6
Eu	....	....	..	2.43	8.6	2.43	8.9
Gd	....	....	..	2.41	7.6	2.41	7.5
Tb	....	....	..	2.39	7.5	2.38	8.0
Dy	2.39	3.08	9	2.37	8.1	2.37	6.8
Er	....	....	..	2.34	7.8	2.34	7.5
Tm	2.33	3.02	8	2.33	8.0	2.33	7.3
Lu	....	....	..	2.31	7.7	2.31	6.8

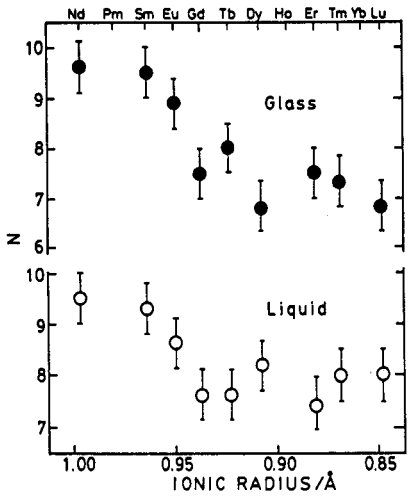

Fig. 7. The hydration number of the lanthanide(III) ions in aqueous perchlorate solutions in the liquid state at room temperature and in the glassy state at liquid nitrogen temperature (12).

The change in the hydration number has also been confirmed from X-ray absorption measurements of perchlorate solutions of a series of lanthanide(III) ions both in the room temperature liquid and in the glassy state at liquid nitrogen temperature. Figure 7 shows clearly the hydration number changes in the middle of the series Sm(III) and Eu(III). The Ln(III)-O distances are in good agreement with those from the neutron diffraction studies. It has been suggested that the equilibrium between eight and nine coordinated species shifts toward the higher hydration state at lower temperature.

The glassy state of electrolyte solutions has shown a surprising structural change. Figure 8 shows the near-edge spectra of aqueous zinc(II) iodide solutions $ZnI_2.RH_2O$ (R=4.7, 10, 20) in liquid and glassy states, and of crystalline powder ZnI_2 and $ZnSO_4.7H_2O$ of known structures. Liquid and glassy samples were measured at room temperature and at liquid nitrogen temperature, respectively. As seen in Fig. 8, in the liquid state the peak at 9670 eV, characteristic for aqua zinc(II) complex, decreases with increasing concentration, whereas the peak at 9663 eV, typical for $[ZnI_4]^{2-}$, increases. These changes in the spectra suggest stepwise formation of zinc(II) iodide complexes in the solutions.

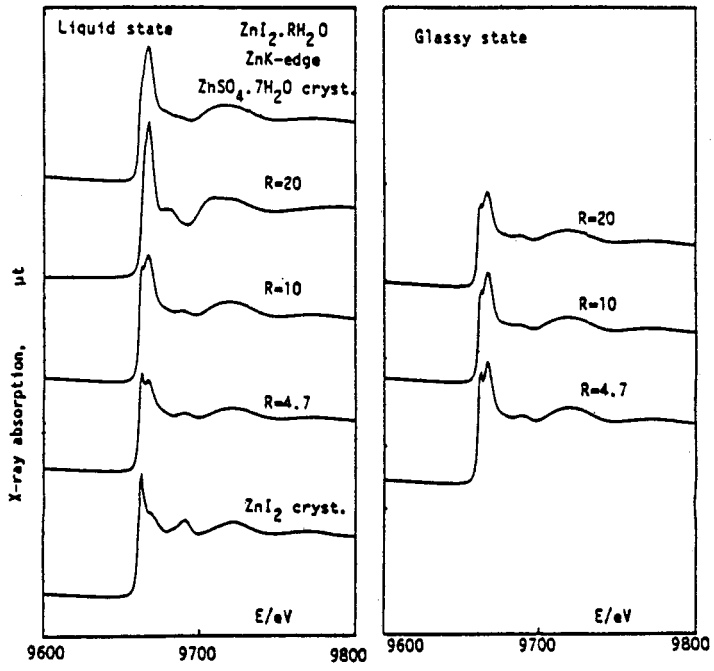

Fig. 8. X-ray absorption near-edge spectra for aqueous solutions of $ZnI_2.RH_2O$ in the liquid state at room temperature and in the glassy state at liquid nitrogen temperature, and for crystalline $ZnSO_4.7H_2O$ and ZnI_2.

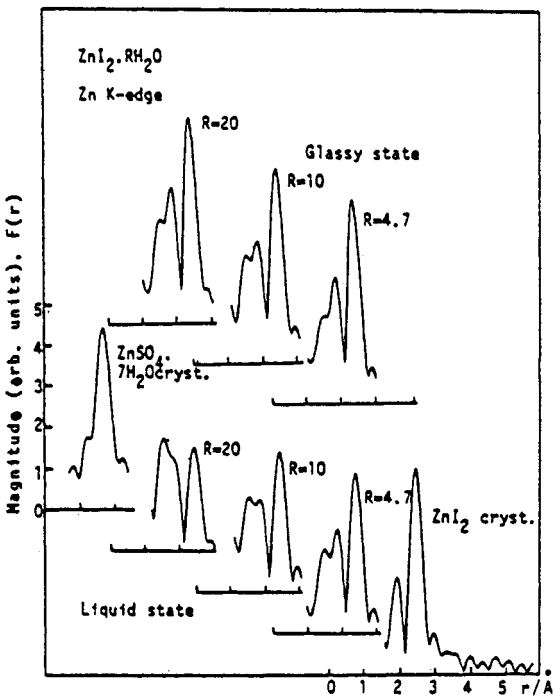

Fig. 9. Fourier transforms for aqueous solutions of $ZnI_2.RH_2O$ in the liquid state at room temperature and in the glassy state at liquid nitrogen temperature, and for crystalline $ZnSO_4.7H_2O$ and ZnI_2.

Table 3. Structural parameters for aqueous solutions of $ZnI_2.RH_2O$ in the liquid state at room temperature and in the glassy state at liquid nitrogen temperature and for crystalline $ZnSO_4.7H_2O$ and ZnI_2

Zn K-edge	Liquid				Glass			
	Zn-I		Zn-O		Zn-I		Zn-O	
	r/Å	N	r/Å	N	r/Å	N	r/Å	N
$ZnI_2.4.7H_2O$	2.56	2.2	1.99	3.2	2.57	2.7	2.04	3.4
$ZnI_2.10H_2O$	2.57	2.2	2.03	2.8	2.58	2.6	2.03	3.0
$ZnI_2.20H_2O$	2.57	1.8	2.03	3.1	2.57	2.5	2.02	3.9
ZnI_2 cryst.	2.58	4*	———					
$ZnSO_4.7H_2O$ cryst.	———		2.08	6*				

* Fixed

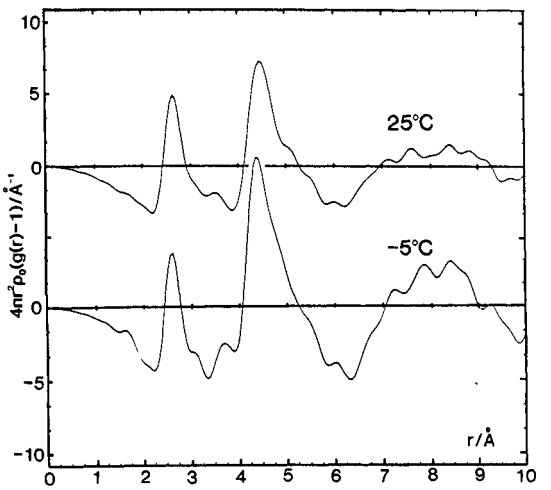

Fig. 10. The total radial distribution functions for aqueous solution of $ZnI_2.5H_2O$ at 25°C and -5°C.

On the other hand, the near-edge spectra in the glassy state show a peculiar trend. For *R*=10 the spectra in the glassy solution are very similar to those in the liquid. However, the equilibrium shifts to form lower complexes for the solution of *R*=4.7, but but to form higher complexes at *R*=20 in the glassy state. Figure 9 shows the Fourier transforms (not corrected for the phase shifts) of the samples investigated. In the solutions at room temperature, the sharp peak at 1.72 Å, ascribed to Zn-OH_2 bonds, decreases and the peak at 2.50 Å due to Zn-I interactions increases with increasing solute concentration, which is consistent with the stepwise complex formation of zinc(II) iodide as suggested from the near-edge spectra. On the contrary, in the glassy state the Fourier transforms of the three solutions are very similar, suggesting the presence of similar species formed in the solutions. The structural parameters obtained are given in Table 3. This structural change in the glassy state can be interpreted in terms of a kind of disproportionation reaction; $2ZnI_2.3H_2O = Zn(OH_2)_6^{2+} + ZnI_4^{2-}$. Similar results have been obtained for zinc(II) chloride and bromide solutions (15,16). This conclusion is consistent with those from Raman spectral measurements (21).

It is interesting to know whether such a disproportionation reaction occurs in an undercooled solution. Total X-ray scatterings from an aqueous solution $ZnI.5H_2O$ have been measured (22). Figure 10 shows the radial distribution functions at room temperature and -5°C. In the radial distribution function the second peak mainly due

to the I···I interactions within tetrahedral zinc(II) iodide complexes increases with the decrease in temperature, but the first peak due to the Zn-I bonds is unchanged. This fact should be interpreted with the formation of higher complexes at -5°C. However, the lower complexes must also be formed to keep the Zn-I peak constant. Thus, the occurrence of the disproportionation reaction is conclusive even in the undercooled state of the solution. Structural determinations of other undercooled solutions are in progress.

CONCLUDING REMARKS

Comparative use of X-ray and neutron diffraction and X-ray absorption techniques has enabled us to determine the structure of electrolyte solutions over a wide range of concentration. The further progress in high intense X-ray sources like synchrotron radiation and pulsed neutron sources will not only improve the quality of data described in this article, but also speed up the measurements and enable critical experiments like those under extreme conditions and time-resolved measurements to study reaction intermediates in solution. We should also bear in mind that the structure of electrolyte solutions should be investigated both from a static feature and from dynamic properties. In this paper the dynamics of ions and water molecules in solutions during supercooling to glass transition process is not mentioned because of a limit of space available. The relaxation time measurements in NMR spectroscopy and quasi-elastic neutron scattering technique give us useful information on dynamic properties of solutions. By looking into solutions from both aspects various physical and chemical phenomena in the solutions will be clarified in detail.

Acknowledgements

The work presented in this paper represents a combined effort of collegues at Fukuoka University in collaboration with National Laboratory of High Energy Physics (KEK, Japan) and Rutherford Appleton Laboratory (RAL, UK). I thank Professor Hisanobu Wakita for his encouragement and discussion, Professor Masaharu Nomura (KEK) for X-ray absorption measurements, Professor Masakatsu Misawa (KEK) and Dr. Alan Soper (RAL) for neutron diffraction measurements. The work was supported by the Grant-in-Aid for Scientific Research No. 635340497, 63044044, and 01540387 from the Ministry of Education, Science, and Culture.

REFERENCES

1. J. Braunstein, Ionic Interactions (I), Academic Press, New York, 1971.
2. T. Yamaguchi, S. Hayashi, and H. Ohtaki, Inorg. Chem., 28, 2434-2439 (1989).
3. H. Ohtaki, Rev. Inorg. Chem., 4, 103 (1982).
4. J. E. Enderby and G. E. Neilson, Rep. Prog. Phys., 44, 38 (1981).
5. D. R. Sandstrom, B. R. Stults, and R. B. Greegor, EXAFS Spectroscopy (Eds. B. K. Teo and D. G. Joy), Plenum Press, New York (1981), Chap. 9, pp. 139-157.
6. K. F. Ludwig, Jr., W. K. Warburth, and A. Fontaine, J. Chem. Phys., 87, 367- (1987).
7. T. Yamaguchi, O. Lindqvist, J. B. Boyce, and T. Claeson, EXAFS and Near Edge Structure III (Eds. K. O. Hodgson, B. Hedmann, and J. E. Benner-Hahn), Springer-Verlag, Berlin,(1984), pp. 417-419.
8. T. Yamaguchi, H. Wakita, and M. Nomura, Photon Factory Activity Report, (in National Laboratory for High Energy Physics, Oho, Tsukuba 305), 6, 28 (1988).
9. S. Ishiguro, B. G. Jeliazkova, and H. Ohaki, Bull. Chem. Soc. Jpn., 58, 1749-1754 (1985).
10. M. Nomura and T. Yamaguchi, J. Phys., Colloque C8, Supp. 12, 47, 619-622 (1986).
11. M. Nomura and T. Yamaguchi, J. Phys. Chem., 92, 6157-6160 (1988).
12. T. Yamaguchi, M. Nomura, H. Wakita, and H. Ohtaki, J. Chem. Phys., 89, 5153-5159 (1988).
13. S. Tanaka, T. Yamaguchi, H. Wakita, and M. Misawa, KENS Report (in National Laboratory for High Energy Physics, Oho, Tsukukuba 305), 7, 49 (1988).
14. T. Yamaguchi, H. Wakita, I. Okada, M. Misawa, A. K. Soper, and S. W. Howlles, ISIS Annual Report (in Rutherford Appleton Laboratory, Chilton, Didcot, Oxon, OX11 0QX, England), p. A55 (1989).
15. T. Yamaguchi, S. Hayashi, and H. Ohtaki, J. Phys. Chem., 93, 2620-2625 (1989).
16. T. Yamaguchi, O. Yata, H. Wakita, and M. Nomura, Photon Factory Activity Report, 5, 230 (1987). ; 6, 46 (1988). ; 6, 47 (1988).
17. T. Yamaguchi, K. Kamihata, H. Wakita, and M. Nomura, Photon Factory Activity Report, 6, 45 (1988).
18. A. H. Narten and R. L. Hahn, J. Phys. Chem., 87, 3193-3197 (1983).
19. B. K. Annis, R. L. Hahn, and A. H. Narten, J. Chem. Phys., 82, 2086-2091 (1985).
20. C. Cossy, A. C. Barnes, J. E. Enderby, and A. E. Merbach, J. Chem. Phys., 90, 3254-3260 (1989).
21. H. Kanno and J. Hiraishi, J. Raman Spectrosc., 9, 85 (1980).
22. T. Yamaguchi, M. Yano, and H. Wakita, Unpublished results.